International Forum on Aeroelasticity and Structural Dynamics
IFASD 2017
25-28 June 2017 Como, Italy

COMPARISON OF NONLINEAR CFD WITH TIME-LINEARIZED CFD AND CFD-CORRECTED DLM FOR GUST ENCOUNTER SIMULATIONS

Christoph Kaiser[1], **Diliana Friedewald**[1], **Jens Nitzsche**[1]

[1]DLR - German Aerospace Center
Institute of Aeroelasticity
Bunsenstr. 10, 37073 Göttingen, Germany
christoph.kaiser@dlr.de

Keywords: aeroelasticity, reduced order model, time-linearized CFD, DLM correction, gust encounter, NASA common research model

Abstract: In this paper the multi-disciplinary simulation of unsteady flight maneuvers is carried out using reduced-order models (ROM) based on Reynolds Averaged Navier-Stokes (RANS) solutions. The analysis of gust encounters on the NASA Common Research model (CRM), a typical transport aircraft configuration, at transonic speed is conducted for two approaches employing time-linearized CFD and CFD-corrected DLM. The results are compared to nonlinear CFD and DLM simulations. The numerical prediction of gust loads requires the coupling of the disciplines aerodynamics, structural dynamics and flight mechanics. The aeroelastic coupling is realized in the frequency domain and in the time domain in terms of generalized coordinates employing a fluid-structure feedback loop.

1 INTRODUCTION

The aircraft load analysis has to be performed for a huge parameter space employing aerodynamic and aeroelastic simulations. Therefore, the computational effort of the numerical methods is crucial. The doublet-lattice method (DLM) [1, 2] is the state-of-the-art method used for predicting unsteady airloads. It is based on the compressible acceleration potential theory for thin wing geometry. Therefore, DLM cannot account for the wing thickness or capture recompression shocks or boundary layer separation.

One approach to overcome the limitations of this method in the transonic regime is to apply a correction of the DLM which allows to introduce information from wind tunnel data or computational methods of higher fidelity. Another approach for the prediction of unsteady airloads is based on the time-linearized Reynolds Averaged Navier-Stokes (RANS) equations as it is implemented in the Linear Frequency Domain (LFD) solver [3] of the DLR TAU-Code. The LFD solver captures the characteristics of the RANS solution while offering a notable reduction in computational effort. Aiming for the aircraft's response to small oscillatory perturbations, the LFD solves for the first harmonic of the flow response.

The frequency-domain approach is well suited for inherently linear problems like the determination of the flutter stability of an aircraft. In contrast, gust simulations are commonly conducted in the time domain in order to account for the large flow perturbations that are caused by gusts. However, by experience, time-linearized gust simulations in most cases can be expected

to yield conservative results. The linearized time-domain gust response is then obtained by the inverse Fourier transform. The time-linearized approach allows the prediction of the dynamic aircraft response on the basis of aerodynamic linear transfer functions that link an excitation to the corresponding aerodynamic force output. Once established these aerodynamic transfer functions can be extended to account for the aircraft's structural dynamic reaction leading to the aeroelastic transfer functions. The applicability of the LFD solver for aerodynamic and aeroelastic gust-encounter simulations is demonstrated by the authors, also for a transport aircraft configuration, in [4, 5].

In this paper, two time-linearized aerodynamic methods based on RANS solutions are presented for predicting unsteady gust loads. On the one hand, the LFD solver is employed for the aircraft's gust encounter and on the other hand, a CFD-based correction method for DLM [6] is applied which is implemented into the in-house tool CREAM (CorREction of Aerodynamic Matrices). This method corrects the frequency-dependent aerodynamic influence coefficients (AIC) of DLM with a few additional RANS solutions at constant frequencies. Both approaches are integrated into a fluid-structure feedback loop in generalized coordinates for the aeroelastic gust responses. The findings are compared to results from uncorrected DLM and from time-marching results with the nonlinear CFD solver of the DLR TAU-Code. The NASA Common Research Model [7] serves as the investigated transport aircraft configuration. Generalized aerodynamic forces and displacements are discussed for small and large gust amplitudes.

2 NUMERICAL METHODS

2.1 Aerodynamic Governing Equations

The DLR TAU-Code [8, 9] is used for solving the Reynolds Averaged Navier-Stokes (RANS) equations with an unstructured finite volume discretization. For unsteady computations the equations are integrated with second-order backward differencing in time employing the dual time stepping approach by Jameson [10]. The turbulence closure used in this paper is the one-equation turbulence model by Spalart and Allmaras [11]. The aerodynamic governing equations are given in integral conservation form for the unknown vector of conservative variables $\mathbf{W}$:

$$\frac{\mathrm{d}}{\mathrm{d}t}\int_{\Omega(t)} \mathbf{W}\mathrm{d}|\Omega| + \mathbf{R}\left(\mathbf{W}, \mathbf{x}, \mathbf{v}_g\right) = 0 \tag{1}$$

$$\mathbf{R}\left(\mathbf{W}, \mathbf{x}, \mathbf{v}_g\right) = \int_{\partial\Omega(t)} \left(\mathbf{f}_{cv} - \mathbf{W}\mathbf{v}_g\right)\cdot\mathbf{n}\mathrm{d}|\partial\Omega| - \int_{\Omega(t)} \mathbf{Q}\mathrm{d}|\Omega| \tag{2}$$

The residual $\mathbf{R}$ consists of the convective and viscous fluxes $\mathbf{f}_{cv}$, the flux from the Arbitrary Lagrangian-Eulerian (ALE) extension [12] and the source term from the turbulence closure. The ALE extension allows moving-grid computations with time-varying grid-node coordinates $\mathbf{x}(t)$. For performing simulations of moving aircrafts, the grid-node coordinates on the aircraft's surface are altered accordingly and the changes are propagated into the volume grid by the help of radial basis functions [13]. The grid-node velocities $\mathbf{v}_g$ result from the time derivative of the grid-node coordinates. Additionally, the grid-node velocities can be exploited to prescribe an independent time-varying velocity field which is denoted as the Field Velocity Method (FVM). The latter is used to directly introduce flow velocities representing a moving gust field [14, 15].

2.2 Linear Frequency Domain Solver

The Linear Frequency Domain (LFD) solver of the DLR Tau-Code allows to solve for the first-harmonic small-disturbance solutions of the RANS equations [3]. The LFD is based on the

discretized governing equations (1) with the integration matrix $\mathbf{V}$:

$$\frac{\mathrm{d}\left(\mathbf{VW}\right)}{\mathrm{d}t} + \mathbf{R}\left(\mathbf{W}, \mathbf{x}, \mathbf{v}_g\right) = 0 \tag{3}$$

For the LFD, the equations are linearized around the steady flow state $\bar{\mathbf{W}}$ by applying the truncated Taylor series expansion. Small harmonic perturbations $\hat{\mathbf{W}}e^{i\omega t}$ of the flow field are presumed which result from small harmonic grid movements of amplitudes $\hat{\mathbf{x}}$ and $\hat{\mathbf{v}}_g$. Under the assumption of a zero steady-state residual, the linearized governing equations are developed in a linear system of equations for the unknown complex-valued first-harmonic amplitudes of the conservative variables:

$$\mathbf{A}\hat{\mathbf{W}} = \mathbf{b} \tag{4}$$

$$\mathbf{A} = i\omega\bar{\mathbf{V}} + \left.\frac{\partial \mathbf{R}}{\partial \mathbf{W}}\right|_{\bar{\mathbf{W}},\bar{\mathbf{x}},\bar{\mathbf{v}}_g} \tag{5}$$

$$\mathbf{b} = -\left(\left.\frac{\partial \mathbf{R}}{\partial \mathbf{x}}\right|_{\bar{\mathbf{W}},\bar{\mathbf{x}},\bar{\mathbf{v}}_g} + i\omega\bar{\mathbf{W}}\left.\frac{\partial \mathbf{V}}{\partial \mathbf{x}}\right|_{\bar{\mathbf{x}}}\right)\hat{\mathbf{x}} - \left.\frac{\partial \mathbf{R}}{\partial \mathbf{v}_g}\right|_{\bar{\mathbf{W}},\bar{\mathbf{x}},\bar{\mathbf{v}}_g}\hat{\mathbf{v}}_g \tag{6}$$

The left-hand side of equation (4) is build up by the analytically derived Jacobian matrix [16] including the turbulence model and depends on the excitation frequency ω. The right-hand side depends on the excitation amplitudes $\hat{\mathbf{x}}$ and $\hat{\mathbf{v}}_g$. It is computed by central finite differences of the residuals of the perturbed flow field. The system of equations is solved iteratively with a Krylov generalized minimum residual scheme (GMRES) [17] and incomplete lower-upper preconditioning [18]. For moving-grid simulations the amplitude of the grid-node velocities are $\hat{\mathbf{v}}_g = i\omega\hat{\mathbf{x}}$. For harmonic gust simulations, the traveling velocity field has to be transformed into the frequency domain yielding $\hat{\mathbf{v}}_g = -\mathbf{w}e^{i\phi(\mathbf{x})}$ with the gust amplitude $\mathbf{w}$ and a spatially dependent phase shift ϕ [4].

2.3 Correction of the Doublet-Lattice Method

The Doublet-Lattice Method (DLM) is based on the compressible acceleration potential theory for a flat-plate geometry in the frequency domain. The matrix of Aerodynamic Influence Coefficients (AIC) relates a harmonic downwash to a harmonic pressure difference for each box of the discretized geometry:

$$\hat{\mathbf{w}} = \mathbf{AIC}(\mathrm{Ma}, \omega)\Delta\hat{\mathbf{c}}_p \tag{7}$$

The AIC matrix is obtained by a Kernel function which depends on the Mach number, the excitation frequency and the distance from one box to another. The downwash vector results from a prescribed harmonic heaving motion of each box. The solution of the linear system yields the harmonic pressure difference which is integrated to obtain the unsteady lifting force for each box.

Since DLM does not cover the effects of viscosity, wing thickness or transonic flow, unsteady results from methods of higher fidelity such as CFD are used to improve the DLM results by a correction of the AIC matrix. In this paper a quasi-steady correction from [6] is applied. Only a single CFD input sample at $\omega_0 = 0$ is needed for the correction. Therefore, a correction matrix is introduced into the system of equations (7) which alters the zeroth order term of the Taylor series expansion of the AIC matrix at ω_0. By replacing the higher order terms of the Taylor

series expansion of AIC matrices at other frequencies with terms from this corrected AIC at $\omega_0 = 0$, the corrected AIC matrices are obtained:

$$\widetilde{\mathbf{AIC}}(\omega) = \mathbf{AIC}(\omega) + (\mathbf{C}_0 - \mathbf{I})\,\mathbf{AIC}(\omega_0) \tag{8}$$

The matrix $\mathbf{C}_0$ is the correction matrix. For the point ω_0, this equation reduces to

$$\widetilde{\mathbf{AIC}}(\omega_0) = \mathbf{C}_0\mathbf{AIC}(\omega_0) \tag{9}$$

which in combination with equation (7) gives the conditional equation for $\mathbf{C}_0$:

$$\hat{\mathbf{w}}(\omega_0) = \mathbf{C}_0\mathbf{AIC}(\omega_0)\Delta\hat{\mathbf{c}}_p(\omega_0) \tag{10}$$

Therefore, the unsteady CFD result has to be geometrically mapped to the DLM discretization in order to obtain the pressure differences at ω_0 for each DLM box. Under the assumption of a diagonal correction matrix, the equation can be solved for the diagonal entries:

$$\mathbf{C}_{0_{ii}} = \frac{\hat{\mathbf{w}}_i(\omega_0)}{\mathbf{AIC}_i(\omega_0)\Delta\hat{\mathbf{c}}_p(\omega_0)} \tag{11}$$

Finally, the following modified system of equations is solved for the corrected DLM:

$$\hat{\mathbf{w}} = \widetilde{\mathbf{AIC}}(\mathrm{Ma}, \omega)\Delta\hat{\mathbf{c}}_p \tag{12}$$

2.4 Aeroelastic Governing Equations

The second-order, linear equations of motion are coupled with the aerodynamic forces in order to perform aeroelastic simulations. The equations of motion are transformed in terms of generalized coordinates which are obtained by a structural modal analysis. The coupled equations are fulfilled for the steady trimmed state. This allows solving the equations only for the dynamic displacements q by removing the the steady state from the equations of motion:

$$\mathbf{M}\ddot{\mathbf{q}}(t) + \mathbf{K}\mathbf{q}(t) = \mathbf{\Phi}^T\mathbf{f}_a(t) = \mathbf{f}_{GAF}(t) \tag{13}$$

The modal mass matrix $\mathbf{M}$ and modal stiffness matrix $\mathbf{K}$ include the rigid body motion and the elastic motion. The aerodynamic forces $\mathbf{f}_a$ are transformed into generalized coordinates by the modal matrix Φ. Therefore, the modal matrix consists of the structural eigenmodes splined to the aerodynamic surface. Equation (13) is integrated in time in a staggered co-simulation applying the Newmark-β method [19] with a predictor-corrector scheme. At each time step, the aerodynamic forces are extrapolated in time in order to predict the modal displacements. These displacements are applied in a moving-grid simulation for solving the aerodynamic forces. The generalized aerodynamic forces (GAF) are used in the corrector step to update the modal displacements and to compute the displacements for the next time step.

By assuming a harmonic motion of the generalized coordinates $\mathbf{q} = \hat{\mathbf{q}}e^{i\omega t}$, equation (13) can be transformed into the frequency domain:

$$-\omega^2\mathbf{M}\hat{\mathbf{q}} + \mathbf{K}\hat{\mathbf{q}} = \mathbf{\Phi}^T\hat{\mathbf{f}}_a = \hat{\mathbf{f}}_{GAF} \tag{14}$$

This equation can be expressed in terms of an aeroelastic feedback loop including a gust excitation as illustrated in the block diagram in Figure 1 and is described in more detail in [5].

The generalized aerodynamic forces of harmonic moving-grid simulations for each generalized coordinate are assembled to build up the GAF matrix for a given frequency. Thus, the columns of the GAF matrix are the force amplitudes $\hat{\mathbf{f}}_{GAF}$ for each generalized coordinate. In order to include the possibility of gust excitation, the GAF matrix is extended by one column with the force amplitude due to harmonic gust encounters. The aeroelastic feedback loop is then solved for the forces and the displacements of the coupled system due to the excitation of a gust encounter. The aeroelastic response is obtained by the convolution of the gust signal with the transfer function of the aeroelastic feedback loop. In the frequency domain, the convolution is computed by multiplication with the Fourier transformed gust signal:

$$\hat{\mathbf{f}}(\omega) = \left(\mathbf{I} - \mathbf{A}\left(\omega\right)\mathbf{S}\left(\omega\right)\right)^{-1}\mathbf{A}\left(\omega\right)\hat{\mathbf{q}}_{gust}\left(\omega\right) \tag{15}$$

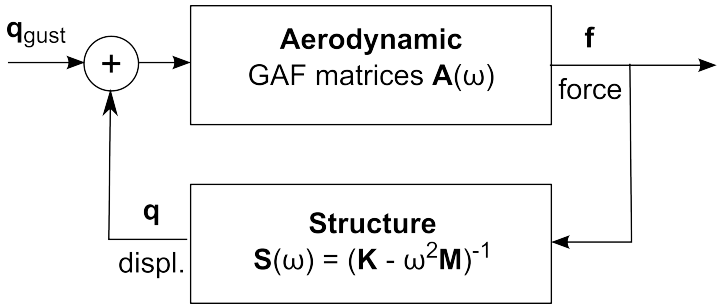

Figure 1: Aeroelastic feedback loop in the frequency domain with gust excitation.

3 RESULTS

3.1 Numerical Setup

The NASA Common Research Model (CRM) [7] is the investigated transport aircraft configuration. The cruise Mach number is 0.86 at an altitude of 9.1 km and the aerodynamic flight shape is trimmed at an angle of attack of 1.641 deg. The steady state is summarized in Table 1.

Parameter	Value
Mach number	0.86
Velocity	260.71 m/s
Angle of attack	1.641 deg
Density	0.4588 $\mathrm{kg/m^3}$
Reynolds number	$56.3 \cdot 10^6$
Reference length	7 m

Table 1: Parameters of the steady flow state.

The aerodynamic model which is used for the computations is based on the publicly available grid from the 4th AIAA Drag Prediction Workshop [20] . The model consists of a wing, a horizontal tailplane (HTP) and a fuselage. A vertical tailplane is not included. The coarse hybrid unstructured-structured volume mesh consists of around 3.7 million points with 100014 surface nodes, see Figure 2(a). The farfield boundary is a hemisphere with a radius of 757 m. Symmetric boundary conditions are defined in the x-z plane in the mid of the fuselage. The surface pressure distribution of the transonic steady state is shown in Figure 2(b). Recompression shocks occur over wide parts of the wing and the HTP. The flow stays fully attached on the configuration.

The DLM discretization for the configuration is shown in Figure 3. The wing is discretized using 20 chordwise boxes resulting in a total number of 800 boxes. In order to obtain a proper

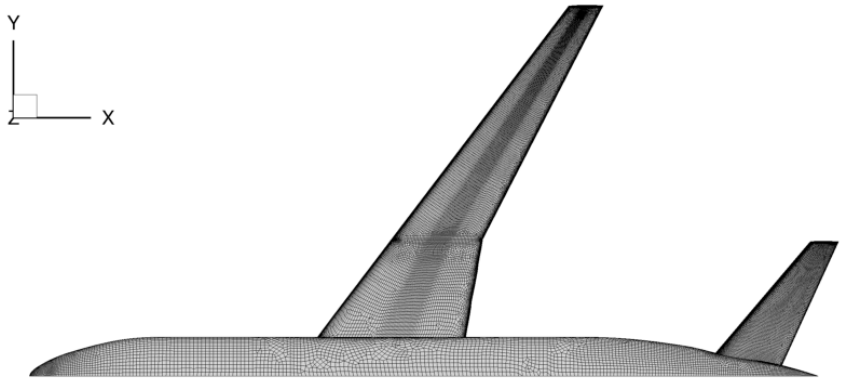

(a) CFD surface grid (top view).

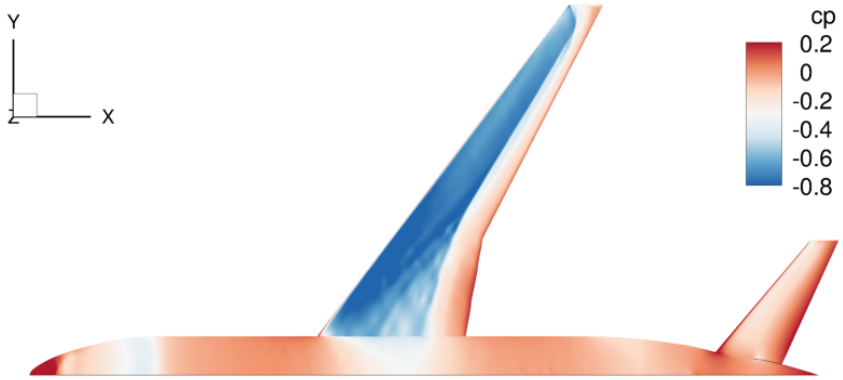

(b) Pressure distribution (top view).

Figure 2: CFD grid and steady flow state of the CRM.

mapping for the DLM correction, the geometry of the CFD and the DLM model needs to be as similar as possible. Therefore, an existing DLM grid [21] of the CRM configuration is modified to include the fuselage. Since the CFD solution changes only little and very smoothly along the fuselage, a coarser discretization than for the wing can be chosen.

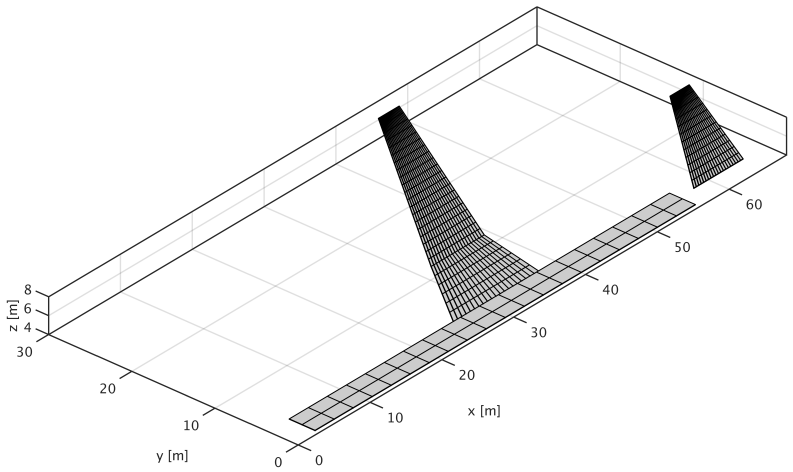

Figure 3: DLM grid of the CRM.

The structural model of the CRM configuration is given in a condensed dynamic form for the

flight state and it is known as the FERMAT model [21]. From the set of the elastic mode shapes, only the first wing bending is included. Additionally, two rigid-body modes are considered, the heave mode and the pitch mode around the center of gravity. These three modes allow describing the primary aircraft response to a vertical gust encounter in symmetric longitudinal flight, which is sufficient for the demonstration of the aeroelastic coupling investigated in this paper. The applied scaling of the three mode shapes and its eigenfrequencies are summarized in Table 2. Since the aerodynamic models in this paper represent only one symmetric half of the CRM, the generalized forces are doubled in the following simulations to match the structural parameters.

Mode	Description	Modal Mass	Eigenfrequency
3	Heave	$2.6 \cdot 10^5$ kg	0.0
5	Pitch	$2.58 \cdot 10^7$ kgm^2	0.0
7	First wing bending	1	1.057 Hz

Table 2: Parameters of the structural model.

Gust encounters as defined by the Certification Specifications for large aeroplanes (CS-25) [22] are listed in Table 3. Two different gust lengths with corresponding amplitudes are considered. The time signals at the nose of the aircraft of both CS-25 gusts are shown in Figure 4.

Parameter	Short gust	Long gust
Amplitude	14.70 m/s	16.94 m/s
Length	91.44 m	213.36 m
Equivalent max. gust angle of attack	3.20 deg	3.72 deg

Table 3: Parameters of the vertical 1-cos gust encounters as defined by CS-25.

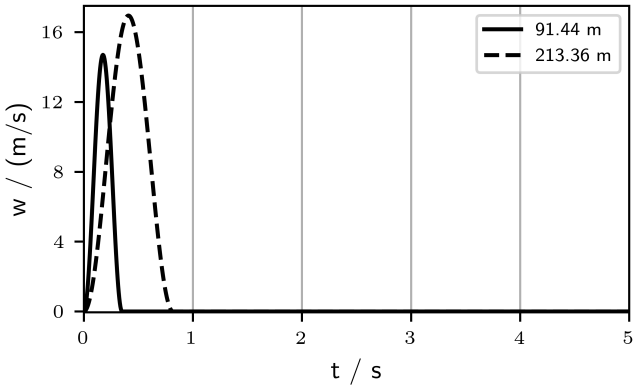

Figure 4: Time signal of the vertical gust velocity at the aircraft's nose.

Due to the large amplitudes of the CS-25 gusts, it is expected that CFD yields nonlinear gust responses. For a validation of the time-linearized approach, small gust amplitudes are considered additionally, in order to ensure an effectively linear response of all methods. These small amplitudes amount to only 5% of the CS-25 gust amplitudes.

3.2 Time-Linearized Aeroelastic Gust Response

The linearized aeroelastic gust response is obtained by employing the aeroelastic feedback loop as described in section 2.4. Therefore, the GAF matrices for a frequency bandwidth are computed with the LFD solver and the CFD-corrected DLM. For saving computational time, the

GAF matrices are computed for a small set of frequencies and the full bandwidth is obtained by interpolation using piecewise monotonic cubic polynomials between the frequency samples. The selected frequency samples cluster at low frequencies and 33 samples are considered. The convolution of the Fourier transformed gust signal with the aeroelastic transfer function, see equation (15), results in the frequency response function (FRF) of the aeroelastic gust response. The FRF is transformed into the time domain by the inverse Fourier transform yielding the time series of the aeroelastic gust response.

Since the investigated methods only affect the aerodynamic results and the structural system remains constant, the aerodynamic response is analyzed in a preliminary step. The transfer function of the aerodynamic system only consists of the GAF matrix which yields the aerodynamic forces due to the gust encounter, see Figure 5.

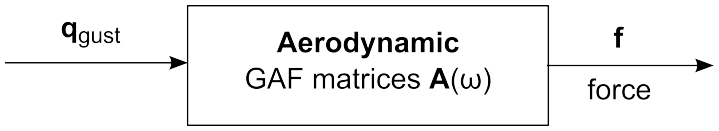

Figure 5: Aerodynamic system in the frequency domain with gust excitation.

In order to guarantee a linear response, the nonlinearly obtained gust responses are computed with a very small gust amplitude. These reference solutions result from aerodynamic and aeroelastic time-domain simulations as described in section 2.1 and 2.4 with gust amplitudes of 5% of the amplitudes defined in the CS-25. The time domain parameters are summarized in Table 4. For the aeroelastic simulation with the Newmark-β method, the time step must be significantly reduced in comparison to aerodynamic simulations in order to avoid numerical instability.

Parameter	Value
Time step size	0.005s / 0.0001s
Number of pseudo iteration	400 / 100
CFL number	25

Table 4: Time-domain simulation parameters for the aerodynamic and aeroelastic reference solutions.

3.2.1 LFD Gust Response

The linearized gust responses obtained with the LFD solver are compared with the nonlinearly obtained reference solution in the time domain. In Figure 6, the aerodynamic forces due to the long and short gust encounter with very small amplitudes are shown. The aerodynamic response is the response of a fixed and rigid aircraft and the gust signal only excites the column corresponding to the harmonic gust forces of the GAF matrix. Thus, the aerodynamic forces are projected onto the structural modes only for visualization. The signals show very good agreement and only very small differences are noticeable at the maximum peaks. The differences can result from either differences between the LFD solution and the nonlinear time-domain solution of the TAU-Code or they may result from the approximation of the FRF by the applied interpolation.

In Figure 7 and Figure 8 the aeroelastic gust responses are shown in the time-domain. The comparison to the reference solution is limited because of the short time signal of the reference solution. Due to the small time step size the computational cost rises very high which has confined the time length of the simulation. Nevertheless, the alignment of the curves at the beginning is very good with little differences. The results for the short gust allow to compare

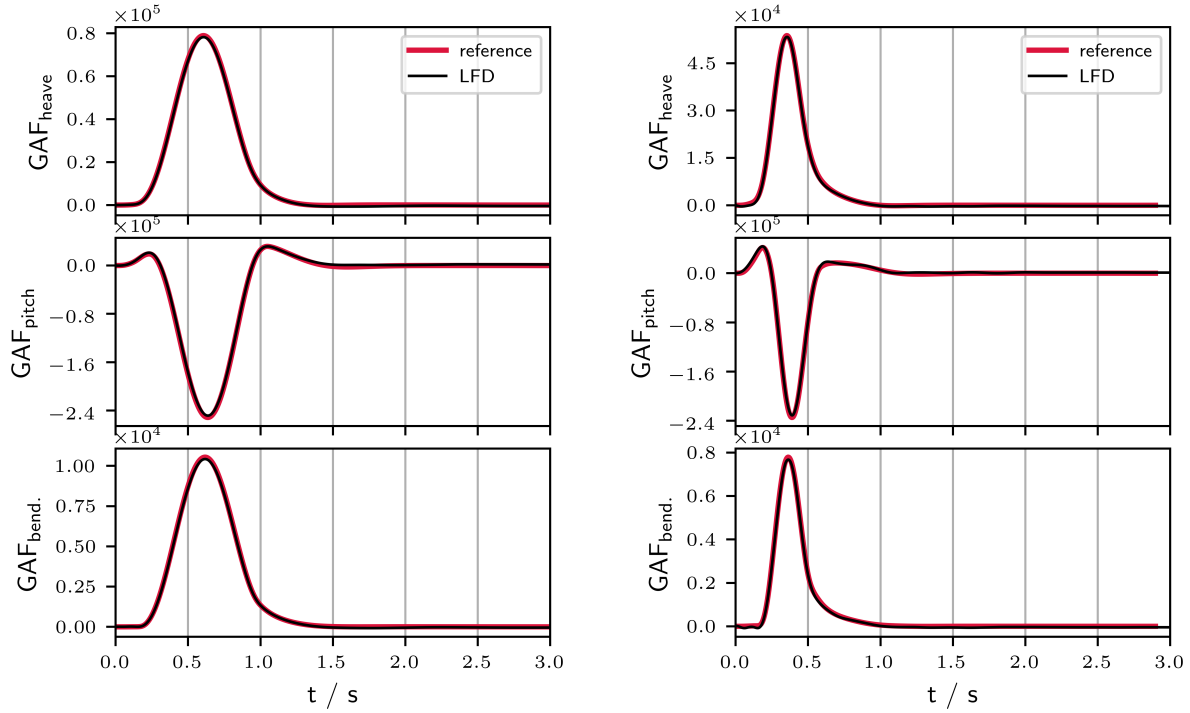

(a) Gust length 213.36 m

(b) Gust length 91.44 m

Figure 6: Time signal of GAFs due to small-amplitude 1-cos gust encounter for a fixed aircraft.

the maximum peaks which agree very well, except for the pitching mode where the LFD result exceeds the reference solution by a small amount. In Figure 8, the movement of the aircraft is visible in terms of modal displacements. The LFD results render a reasonable motion. The heave degree of freedom experiences a permanent offset while the other displacements return to zero. The pitch degree of freedom performs a mainly negative movement which results from the longitudinal stability of the aircraft.

3.2.2 CFD-Corrected DLM Gust Response

The gust responses obtained with the CFD-corrected DLM are on the one hand compared to results from the LFD solver and on the other hand to results from the uncorrected doublet-lattice method. The input for the correction method used here is a single LFD solution for a pitching motion at zero frequency. In Figure 9, one entry of the GAF matrix is shown for the three investigated aerodynamic methods. This entry corresponds to the lift force due to the gust excitation and it shows the effect of the quasi-steady correction method. At zero frequency, the DLM result is corrected with CREAM to match the gust response of the LFD which yields from the resemblance of the gust mode with the pitch mode at zero frequency. For frequencies above 0.5Hz, CREAM and LFD start to deviate. Note that also the imaginary part of the corrected GAF matrix is changed, although the modification is based on a real-valued input sample only. Similar results using the same correction method for a fixed aircraft can be found in [23].

The time-domain results for the long and short gust encounter are depicted in Figure 10. Especially for the long gust, the improvement of the doublet-lattice correction is obvious, since LFD and CREAM show only little difference in their GAFs for heave and bending. In contrast, the uncorrected DLM underpredicts the LFD peaks of both generalized forces. Some deviations can be noticed in the time signal for the pitch GAF. Compared to LFD, CREAM results

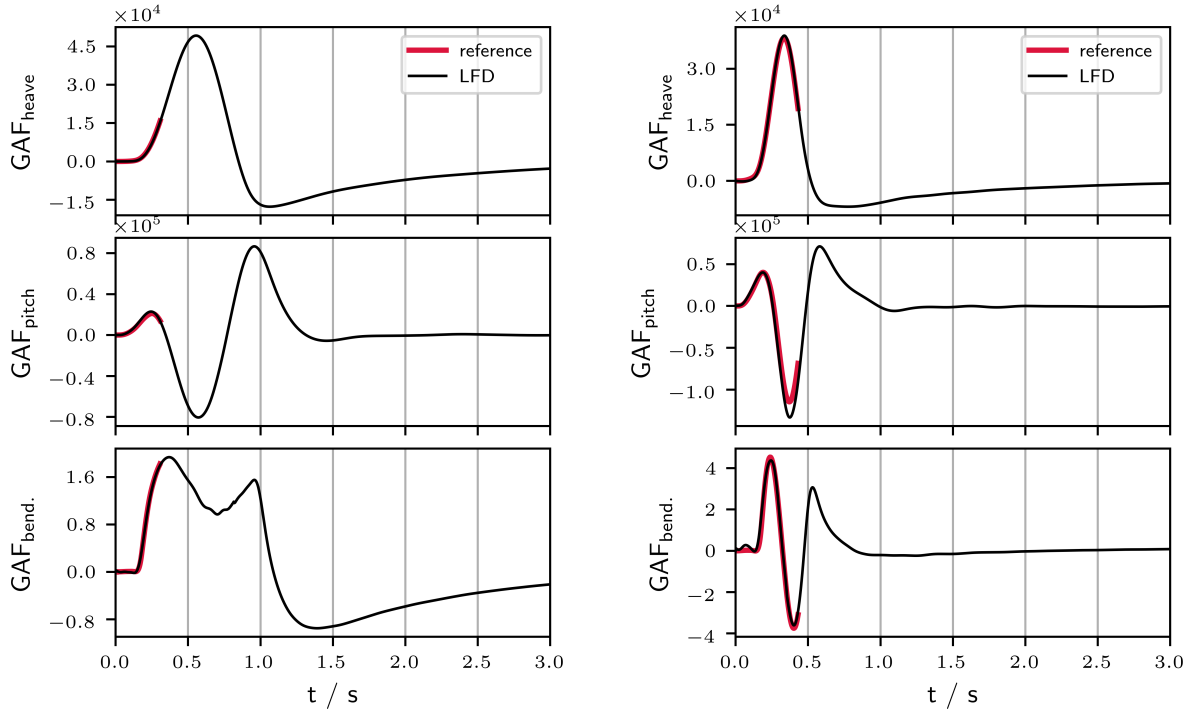

(a) Gust length 213.36 m (b) Gust length 91.44 m

Figure 7: Time signal of GAFs due to small-amplitude 1-cos gust encounter.

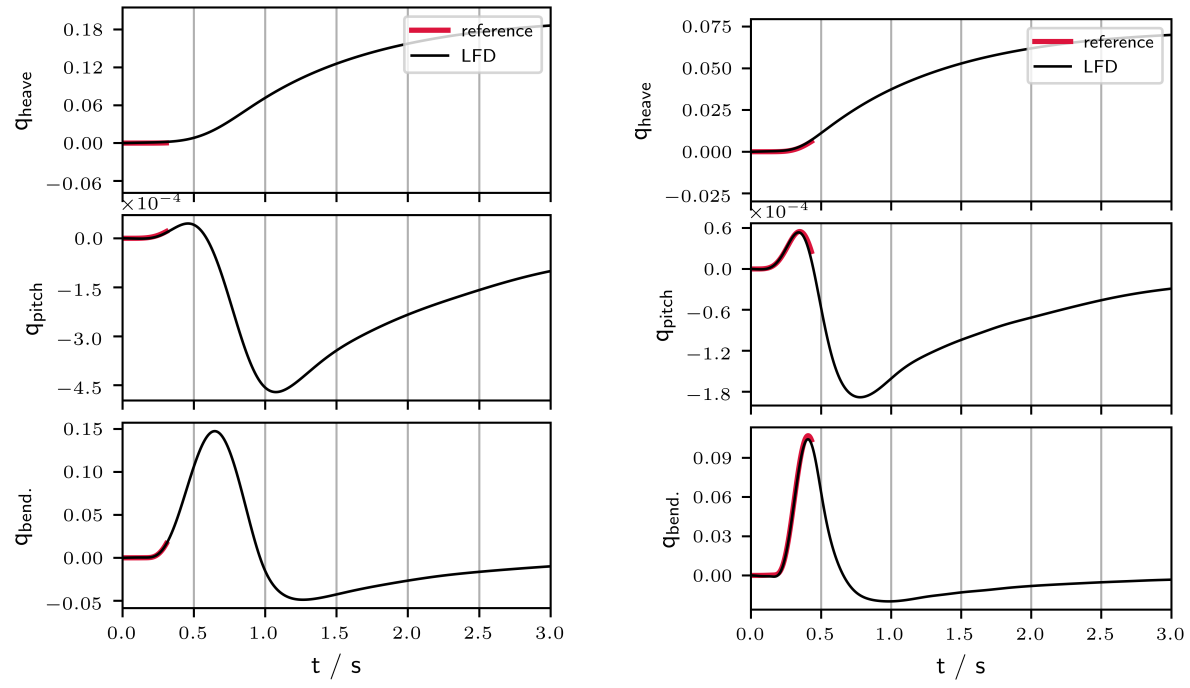

(a) Gust length 213.36 m (b) Gust length 91.44 m

Figure 8: Time signal of modal displacements due to small-amplitude 1-cos gust encounter.

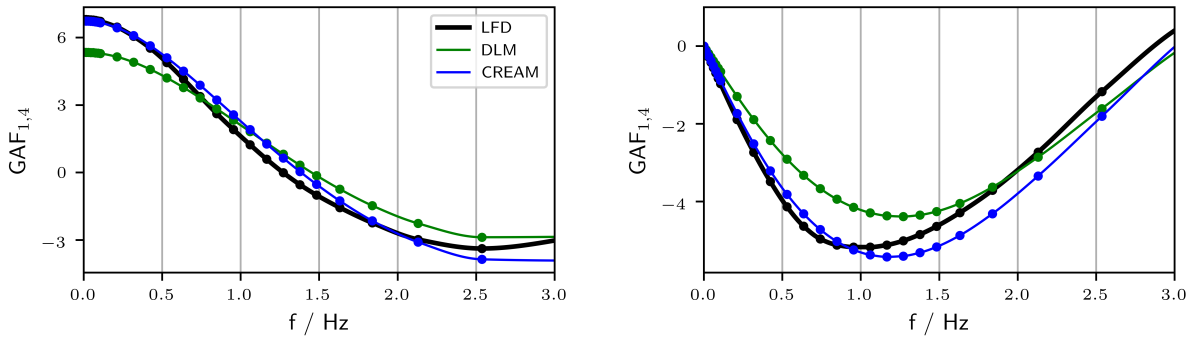

(a) real part (b) imaginary part

Figure 9: Harmonic gust force projected onto the heave mode for a fixed aircraft.

in a slightly stronger oscillation in the beginning of the signal, and in a too strongly damped signal after the gust encounter. The generalized forces due to the short gust encounter show similar trends, though in this case, the correction method tends to overpredict the peak loads slightly. The short gust excites a broader frequency spectrum than the long gust. Hence, due to the deviations of CREAM and LFD for higher frequencies, the agreement between the methods improves with increasing gust length, see also [23].

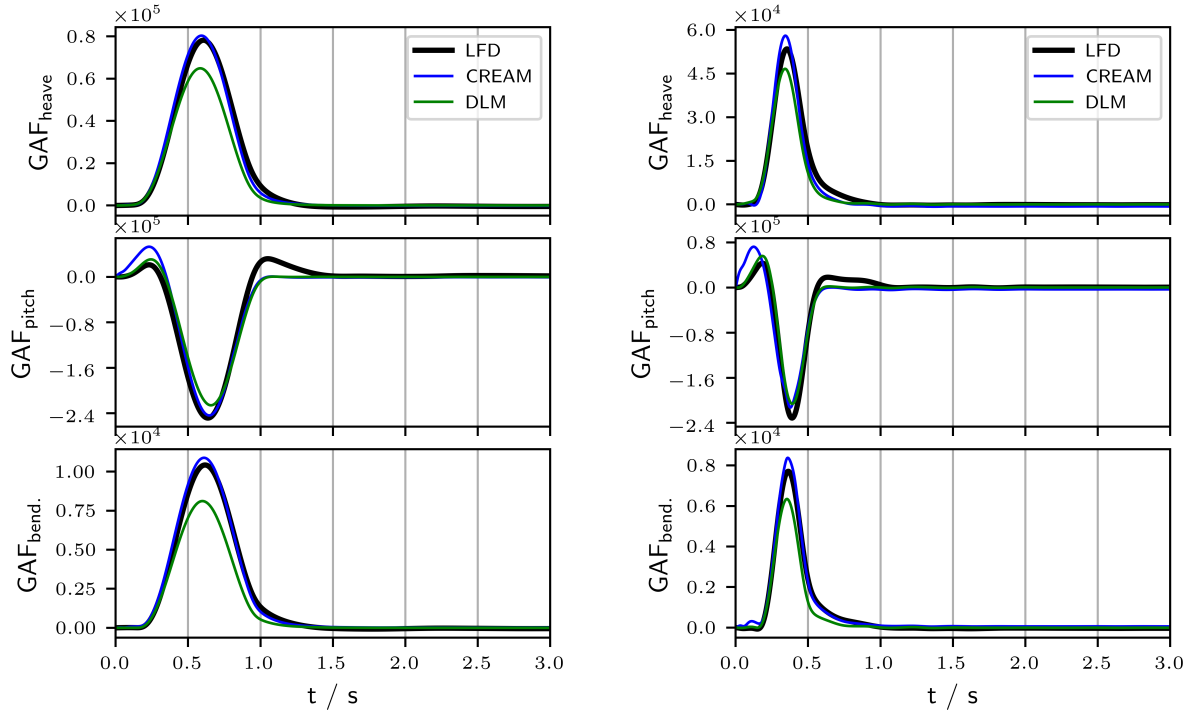

(a) Gust length 213.36 m (b) Gust length 91.44 m

Figure 10: Time signal of GAFs due to small-amplitude 1-cos gust encounter for a fixed aircraft.

The time signals of the aeroelastic GAFs and modal displacements for the long gust are depicted in Figure 11. Compared to the aerodynamic responses in Figure 10, the structural coupling introduces additional oscillations into the responses. This indicates that the GAF matrix obtained by CREAM is more sensitive to the interpolation between the selected frequency samples than for DLM or LFD.

The modal displacements for all three mode shapes shows a better match for DLM and LFD than for CREAM. For heave and pitch, the results deviate shortly after the maximum gust velocity is reached, compare with Figure 4, at about 0.5s. The first peak of the time signal from the bending motion is captured very well by CREAM, but as in the aerodynamic computations, the response seems to strongly damped.

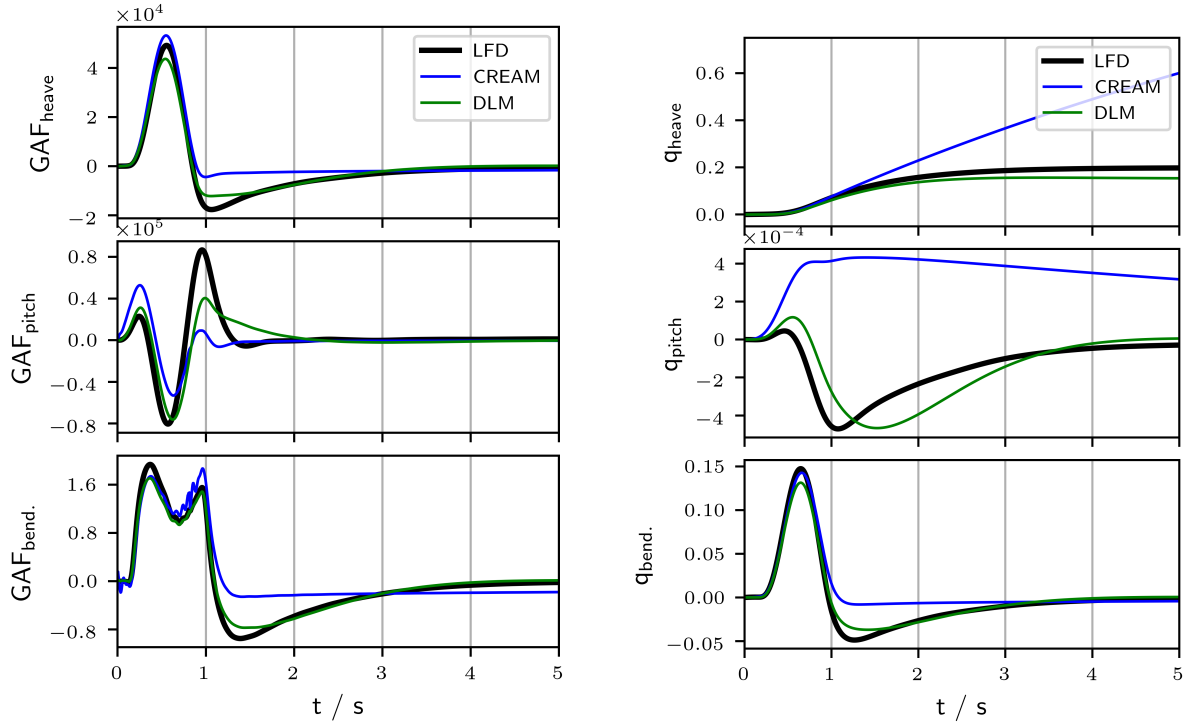

(a) GAFs (b) modal displacements

Figure 11: Time signals of small-amplitude 1-cos gust encounter with gust length of 213.36 m.

3.3 Nonlinear Aeroelastic Gust Response

The gust analysis as defined in the CS-25 demands gust amplitudes which exceeds the range of linear responses. In this section, the time-linearized aerodynamic and aeroelastic gust responses obtained with the LFD solver are compared to the nonlinear gust responses for analyzing the applicability of the time-linearized approach for CS-25 gusts. In Figure 12 the aerodynamic forces are shown for the fixed aircraft. Significant deviations in the peaks and in the temporal behavior can be observed. The nonlinear forces are attenuated but exhibit a more oscillatory progression. This trend is more distinct for the large gust. However, the results suggest that the time-linearized approach yields a conservative estimation of the aerodynamic loads due to gust encounters. Figure 13 displays the aeroelastic gust response for the small gust. For both the forces and the displacements differences are observable. However, they tend to be less than for the fixed aircraft which is more distinct for the modal displacements. A significant difference is noticeable in the GAF of the bending mode. The nonlinear force exceeds the time-linearized result by a factor of two. This is noteworthy since the time-linearized bending force is no longer a conservative estimate.

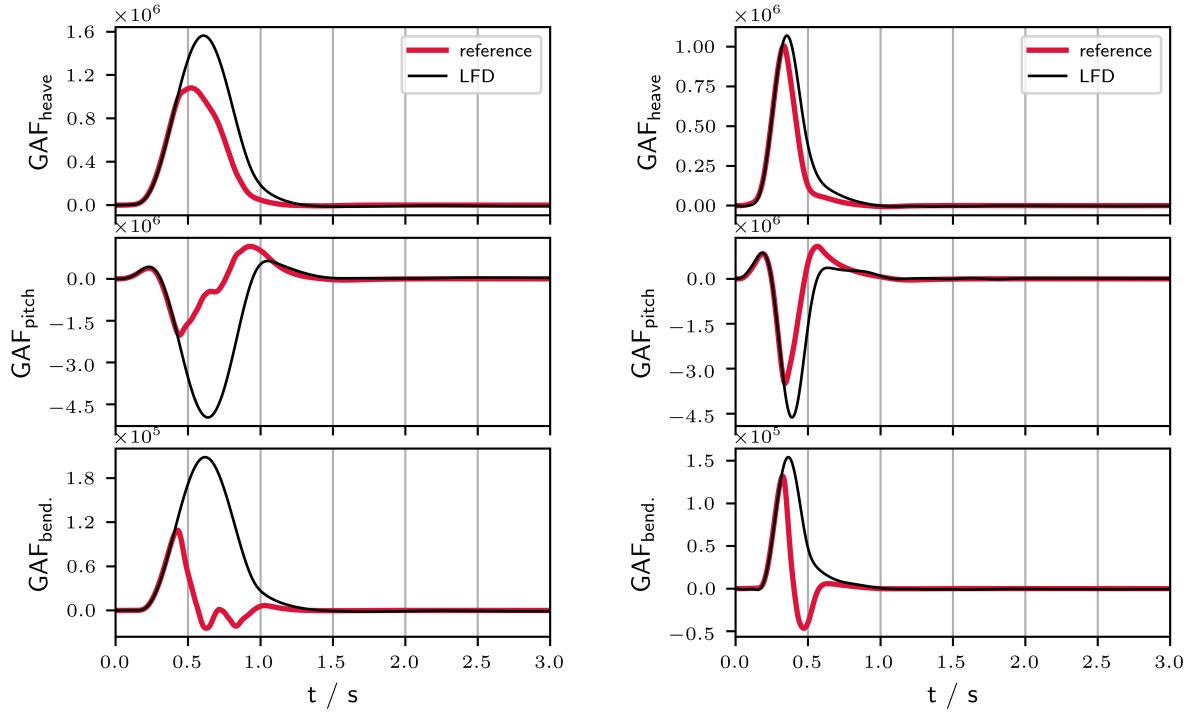

(a) Gust length 213.36 m (b) Gust length 91.44 m

Figure 12: Time signal of GAFs due to 1-cos gust encounter from CS-25 for a fixed aircraft.

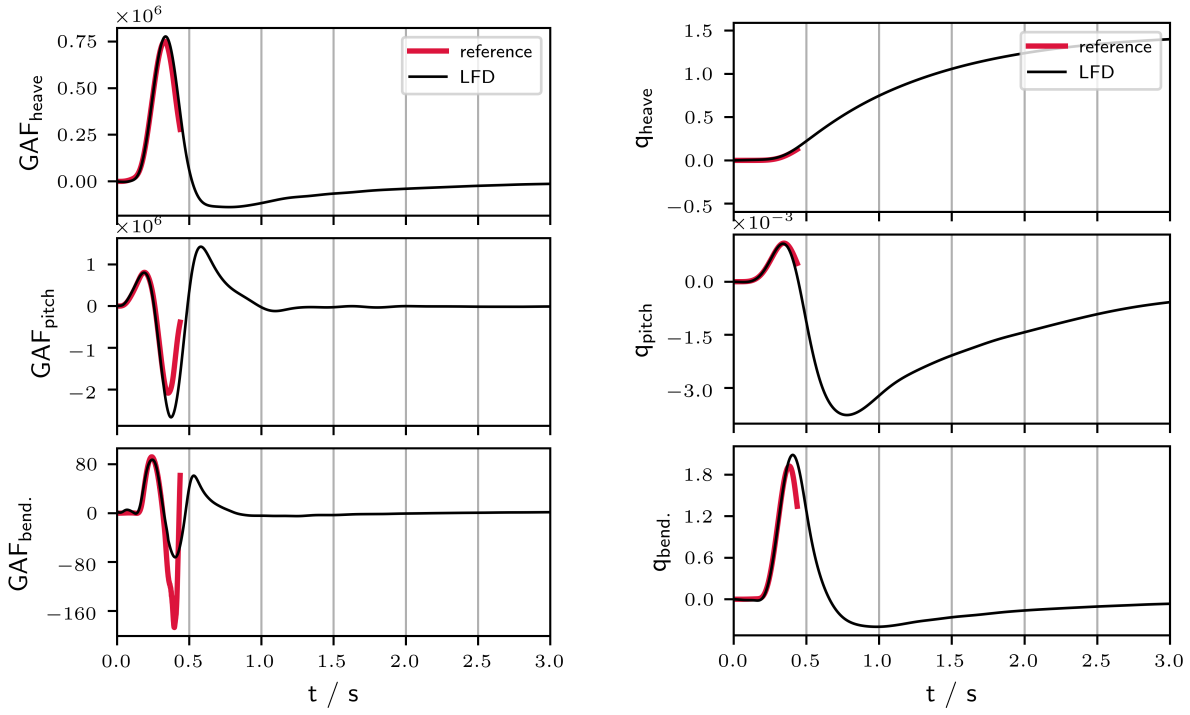

(a) GAFs (b) modal dsiplacements

Figure 13: Time signal of GAFs due to 1-cos gust encounter from CS-25 with gust length of 91.44 m.

4 CONCLUSION

In this paper, two time-linearized aerodynamic methods based on RANS solution are presented for predicting unsteady gust loads. Aeroelastic simulations for the CRM aircraft including two rigid body modes and one flexible mode are performed in the frequency domain and transformed into the time domain. The gust responses are compared to nonlinearly obtained time-domain solutions demonstrating the feasibility of the reduced-order models.

Very good agreement is achieved for the LFD-based ROM in the linear gust regime. For gust amplitudes as defined by the CS-25 strong nonlinear responses are received which yields to attenuated aerodynamic forces and the LFD solver overpredicts the gust loads. Similar results are obtained by comparison of CFD and DLM [24]. However, the aeroelastic results also show an underpreditction of the forces on the first wing bending mode. The CFD-corrected DLM results show promising aerodynamic loads due to gust encounters. Nevertheless, the results of the aeroelastic responses are not suitable indicating that a quasi-steady correction is not sufficient for aeroelastic coupled simulations.

Considering the computational cost the LFD-based ROM required 33 computations by the LFD solver which exceeds the effort for one nonlinear aerodynamic time-domain simulation by a factor of three. However, the same results can be utilized for many gust cases and long periods of time. They can also be exploited for further linear aeroelastic analysis. The nonlinear aeroelastic time-domain simulation demands much more computational effort which is illustrated by the displayed time periods of small length. By contrast, the CFD-corrected DLM required only one LFD solution whereas the computational cost of the DLM results are negligible in comparison to CFD.

Finally, four different aerodynamic methods are analyzed for predicting aeroelastic loads on a transport aircraft configuration for gust encounters as defined by the CS-25.

5 ACKNOWLEDGMENTS

This work was supported by the AEROGUST project which has received funding from the European Unions Horizon 2020 research and innovation programme under grant agreement No 636053. The partners in AeroGust are: University of Bristol, INRIA, NLR, DLR, University of Cape Town, NUMECA, Optimad Engineering S.r.l., University of Liverpool, Airbus Defence and Space, Dassault Aviation, Piaggio Aerospace and Valeol.

6 REFERENCES

[1] Albano, E. and Rodden, W. P. (1969). A doublet-lattice method for calculating lift distributions on oscillating surfaces in subsonic flows. *AIAA Journal*, 7(2), 279–285. doi: 10.2514/6.1968-73.

[2] Blair, M. (1992). A compilation of the mathematics leading to the doublet lattice method. Tech. rep.

[3] Thormann, R. and Widhalm, M. (2013). Linear-Frequency-domain predictions of Dynamic-Response data for viscous transonic flows. *AIAA Journal*, 51(11), 2540–2557.

[4] Kaiser, C., Thormann, R., Dimitrov, D., et al. (2015). Time-Linearized Analysis of Motion-induced and Gust-induced Airloads with the DLR TAU Code. In *Deutscher Luft- und Raumfahrtkongress*.

[5] Kaiser, C., Friedewald, D., Quero-Martin, D., et al. (2016). Aeroelastic Gust Load Prediction based on time-linearized RANS solutions. In *Deutscher Luft- und Raumfahrtkongress*. DocumentID: 420161.

[6] Thormann, R. and Dimitrov, D. (2014). Correction of aerodynamic influence matrices for transonic flow. *CEAS Aeronautical Journal*, 5(4), 435–446. ISSN 1869-5582. doi: 10.1007/s13272-014-0114-3.

[7] Vassberg, J., Dehaan, M., Rivers, M., et al. (2008). Development of a Common Research Model for Applied CFD Validation Studies. In *Guidance, Navigation, and Control and Co-located Conferences*. American Institute of Aeronautics and Astronautics. doi: 10.2514/6.2008-6919.

[8] Gerhold, T., Galle, M., Friedrich, O., et al. (1997). Calculation of complex three-dimensional configurations employing the DLR-TAU-code. In *35th Aerospace Sciences Meeting and Exhibit*. doi:10.2514/6.1997-167.

[9] Schwamborn, D., Gerhold, T., and Heinrich, R. (2006). The DLR TAU-code: Recent applications in research and industry. In *European Conference on Computational Fluid Dynamics (ECCOMAS)*.

[10] Jameson, A. (1991). Time dependent calculations using multigrid, with applications to unsteady flows past airfoils and wings. In *10th Computational Fluid Dynamics Conference*. doi:10.2514/6.1991-1596. AlAA 91-1596.

[11] Spalart, P. and Allmaras, S. (1992). A one-equation turbulence model for aerodynamic flows. In *30th Aerospace Sciences Meeting and Exhibit*. doi:10.2514/6.1992-439. AIAA-92-0439.

[12] Hirt, C., Amsden, A. A., and Cook, J. L. (1974). An Arbitrary Lagrangian-Eulerian Computing Method for All Flow Speeds. *Journal of Computational Physics 14*, 227–253.

[13] de Boer, A., van der Schoot, M. S., and Bijl, H. (2007). Mesh deformation Based on Radial Basis Function Interpolation. *Computers and Structures*, 85(2), 784–795.

[14] Singh, R. and Baeder, J. D. (1996). The direct calculation of indicial lift response of a wing using computational fluid dynamics. In *AIAA Applied Aerodynamics Conference*.

[15] Heinrich, R. (2014). Simulation of Interaction of Aircraft and Gust Using the TAU-Code. In *New Results in Numerical and Experimental Fluid Mechanics IX*, vol. 124 of *Notes on Numerical Fluid Mechanics and Multidisciplinary Design*. Springer International Publishing, pp. 503–511.

[16] Dwight, R., Brezillon, J., and Vollmer, D. B. (2006). Efficient Algorithms for Solution of the Adjoint Compressible Navier-Stokes Equations with Applications. In *7th ONERA-DLR Aerospace Symposium (ODAS)*.

[17] Saad, Y. and Schultz, M. H. (1986). GMRES: A Generalized Minimun residual Algorithm for Solving Nosymmetric Linear Systems. *SIAM Jounral on Scientific and Statistical Computing*, 7(3), 856–859.

[18] McCracken, A. J., Timme, S., and Badcock, K. . J. (2012). Accelerating Convergence of the CFD Linear Frequency Domain Method by a Preconditioned Linear Solver. In *6th European Congress on Computational Mathematics in Applied Sciences and Engineering (ECCOMAS)*.

[19] Newmark, N. M. (1959). A method of computation for structural dynamics. *Journal of Engineering Mechanics, Proceedings of the American Society of Civil Engineers*, 85, (EM3), 67–94.

[20] 4th AIAA Drag Prediction Workshop (2017). ftp://cmb24.larc.nasa.gov/outgoing/dpw4/dlr/solargrids.

[21] Klimmek, T. (2014). Parametric Set-Up of a Structural Model for FERMAT Configuration for Aeroelastic and Loads Analysis. *Journal of Aeroelasticity and Structural Dynamics*, 3(2), 31–49.

[22] European Aviation Safety Agency (EASA) (2012). Certification specifications and acceptable means of compliance for large aeroplanes CS-25, amendment 12. Tech. rep., European Aviation Safety Agency (EASA).

[23] Friedewald, D., Thormann, R., Kaiser, C., et al. Quasi-Steady Doublet-Lattice Correction for Aerodynamic Gust Response Prediction in Attached and Separated Transonic Flow. *CEAS Aeronautical Journal*. Currently under review.

[24] Reimer, L., Ritter, M., Heinrich, R., et al. (2015). CFD-based Gust Load Analysis for a Free-flying Flexible Passenger Aircraft in Comparison to a DLM-based Approach. In *22nd AIAA Computational Fluid Dynamics Conference*. AIAA 2015-2455.

COPYRIGHT STATEMENT